Title; Effect of Fine-Grained Area's Dissolution after Solution Treatment on Tensile and Creep Life Enhancement of Hot Rolled Rene 65

M. Safavi[1], M. R. Aboutalebi[2], S.M. Abbasi[3], S.H. Razavi[4]

[1] PHD Student, IUST of Iran. Email: Mehdi_safavi@iust.ac.ir- [2] Professor, IUST of Iran. Email: mrezab@iust.ac.ir- [3] Professor, MUT of Iran. Email: SMA_abbasi@yahoo.com [4] Associated Professor, IUST of Iran. Email: Hrazavi@iust.ac.ir

Abstract

The effect of solution-treatment temperature on the dissolution of fine-grained areas (FGAs), γ′ precipitation, and high-temperature mechanical behavior of hot-rolled René 65 was investigated. Solution treatments were performed at 1055–1115 °C for 2 h, followed by air cooling and aging at 760 °C for 8 h. Increasing solution temperature progressively reduced the FGA fraction and promoted a more homogeneous γ′ distribution, while excessive treatment at 1115 °C resulted in pronounced grain growth and precipitate coarsening. The 1095 °C condition provided the most favorable microstructural balance, with substantially reduced FGA-related heterogeneity, improved tensile ductility, and the lowest measured minimum creep rate. Under creep testing at 730 °C/530 MPa, the 1095 °C specimen remained unfailed beyond 100 h and was therefore classified as a run-out condition. These results indicate that controlling FGA dissolution while limiting grain growth is critical for optimizing the high-temperature performance of hot-rolled René 65.

Keywords: René 65 superalloy, fine-grained areas (FGAs), solution treatment, γ' precipitates, creep resistance.

1. Introduction

Nickel-based superalloys are essential for aero-engine turbine disks due to their excellent creep resistance and dimensional stability at high temperatures [1,2]. René 65 is a relatively new cast-and-wrought alloy introduced as a more economical replacement for René 88DT in components such as disks and rings for the latest LEAP engines [3,4]. One of its main advantages over powder metallurgy alloys is the combination of good workability and a high γ' volume fraction, typically 40–50% [4,5]. The mechanical properties of René 65 depend heavily on the size, distribution, and morphology of primary (γ'I), secondary (γ'II), and tertiary (γ'III) γ' precipitates [1,2,8]. Coarse γ′I particles, commonly located at grain boundaries, restrict grain-boundary migration and limit grain growth during heat

[DOI: 10.22068/ijmse.4669]

treatment, whereas the finer γ′II and γ′III precipitates formed during cooling and aging provide matrix strengthening by impeding dislocation motion [6,7,9]. Hot deformation can also generate local regions of high stored strain and dislocation density when recrystallization is incomplete, contributing to microstructural heterogeneity and the development of fine-grained regions after subsequent sub-solvus treatment [3,9,10]. Solution-treatment temperature is therefore a critical parameter because it controls the extent of primary γ′ dissolution, grain-boundary mobility, final grain size, and the precipitation response during subsequent cooling and aging [5,10,12]. Sub-solvus treatments retain a fraction of primary γ′ that restricts grain growth, whereas treatments approaching or exceeding the γ′ solvus promote greater dissolution and matrix supersaturation but increase the risk of rapid grain coarsening [8]. Although several studies have examined René 65, there is still limited information on how best to remove the deformation-induced FGAs that appear after hot rolling while maintaining good tensile and creep properties [3,11-12]. The present work therefore focuses on solution treatments between 1055 °C and 1115 °C applied to hot-rolled material, with the aim of identifying practical conditions that homogenize the microstructure and improve high-temperature performance for turbine disk applications.

2. Experimental Procedure

The material used in this study was produced by vacuum induction melting (VIM) followed by electroslag remelting (ESR) in the form of 90 mm diameter ingots. The chemical composition of the investigated René 65 alloy is presented in Table 1. Prior to hot working, the ESR ingots were homogenized in two stages, at 1100 °C for 5 h followed by 1150 °C for 5 h. Hot rolling was subsequently performed at 1150 °C in seven passes, producing a total thickness reduction of approximately 70%, from 34 mm to 8.5 mm. Samples for DSC analysis, metallographic characterization, tensile testing, and creep testing were machined from the hot-rolled strip.

Differential scanning calorimetry was carried out using a TA Instruments SDT 650 at a heating rate of 10 °C/min to determine the γ′ dissolution and precipitation temperature ranges [3]. Based on the DSC results, solution treatments were conducted at 1055, 1075, 1095, and 1115 °C for 2 h, followed by air cooling. All specimens used for microstructural characterization, tensile testing, and creep testing were subsequently aged at 760 °C for 8 h [3,5]. Microstructural observations were performed using an Olympus BX51 optical microscope and a TESCAN MIRA3 FESEM equipped with EDS. Samples were

[DOI: 10.22068/ijmse.4669]

prepared by electropolishing and electro-etching using a solution containing 40 ml HCl, 30 ml HNO_3, and 30 ml H_2O. Grain size, γ′ volume fraction, and precipitate size were evaluated using ImageJ. Grain size and γ′ volume fraction were determined from three independent measurements, and the corresponding error bars represent the standard deviation of these measurements. Hardness measurements were performed separately in the matrix and FGA regions using an INNOVATEST microhardness tester with a 0.3 kgf load, with 3–5 measurements taken for each condition.

Tensile tests were conducted at 650 °C and a strain rate of 0.1 s^{-1} using an Instron 8500 series testing system. Creep tests were performed at 730 °C under an applied stress of 530 MPa using plate-type specimens in a dead-weight creep testing machine equipped with an external extensometer. A run-out criterion of more than 100 h was adopted for the creep tests. If a specimen remained un-failed and had not entered the tertiary creep stage beyond this duration, the test was terminated and classified as a run-out condition. For such specimens, the creep strain at test termination was reported as the final experimental result. DSC and creep tests were performed once for each condition; therefore, the creep results are interpreted as comparative experimental observations rather than statistically validated rupture-life data.

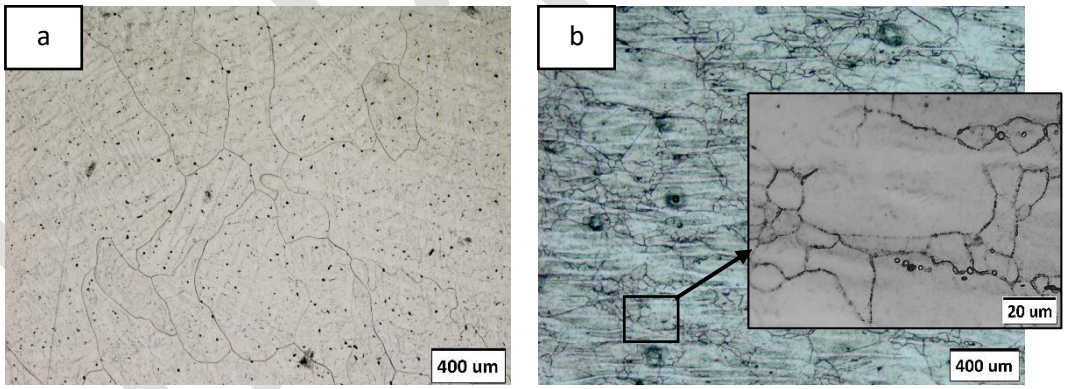

Fig. 1. (a) Microstructure of the homogenized VIM+ESR Rene 65 superalloy; (b) microstructure after hot rolling.

3. Results and Discussion

3.1 Initial Microstructure and Solution Treatment Temperatures

The homogenized VIM+ESR René 65 superalloy exhibited a coarse-grained structure with an average grain size exceeding 1000 μm. Hot rolling produced significant grain refinement to approximately 29 μm, accompanied by a necklace-type microstructure consisting of fine recrystallized grains (5–15 μm) surrounding larger unrecrystallized grains, along with pronounced wavy shear bands (Fig. 1). These

[DOI: 10.22068/ijmse.4669]

shear bands resulted from intense plastic deformation and incomplete dynamic recrystallization (DRX) and post-dynamic recrystallization (PDRX) during thermomechanical processing. In γ′-strengthened nickel-based superalloys, deformation is typically accommodated by dynamic recovery and DRX, with γ' precipitates promoting distributed deformation through particle pinning of grain boundaries rather than severe strain localization [8,9]. The persistence of shear bands in the present material indicates incomplete recrystallization, creating high-dislocation-density regions that serve as fast diffusion paths and preferential nucleation sites for γ' precipitation during subsequent heat treatments.

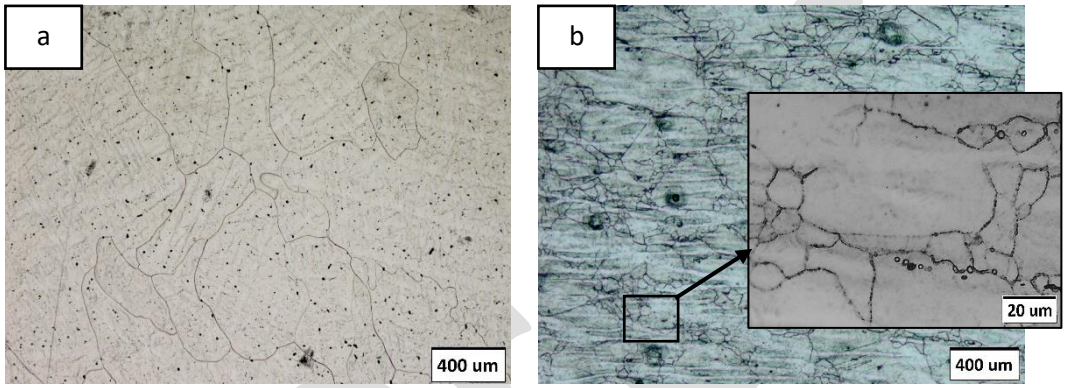

Fig. 1. (a) Microstructure of the homogenized VIM+ESR Rene 65 superalloy; (b) microstructure after hot rolling.

Differential scanning calorimetry (DSC) of the hot-rolled alloy revealed the onset of γ' dissolution at approximately 1075 °C during heating and an exothermic peak for γ' precipitation at 1055–1056 °C during cooling (Fig. 2). This dissolution onset is lower than values reported for VIM+ESR+VAR (triple melted) processed René 65 (≈1110 °C) [3,13], likely due to differences in solidification history, elemental segregation, and minor variations in Al and Ti content. Similar sensitivity of the γ' solvus to processing route and composition has been noted in related alloys such as AD730 [14].

[DOI: 10.22068/ijmse.4669]

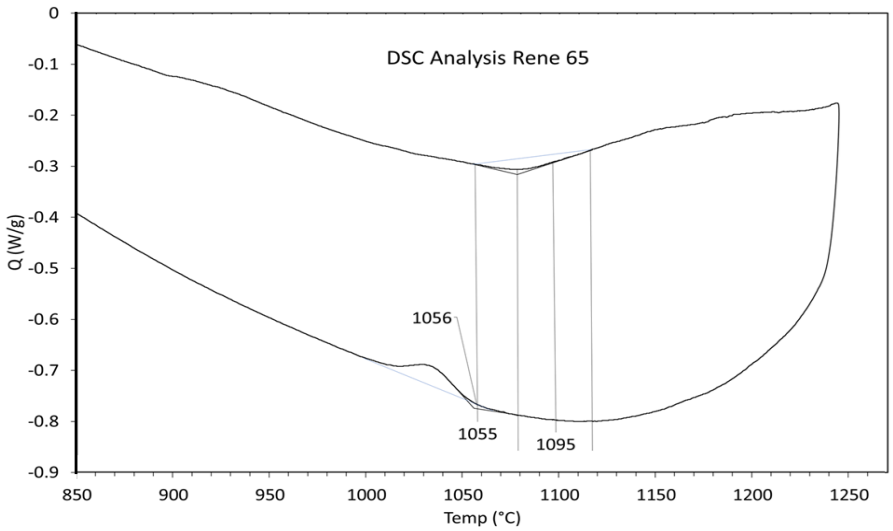

Fig. 2. DSC thermogram of the hot-rolled Rene 65 superalloy showing the experimentally determined γ′ dissolution and precipitation temperatures and the selected solution treatment temperatures.

Solution treatments were therefore performed in the 1055–1115 °C range to encompass sub-solvus and super-solvus conditions relative to the experimentally determined γ' solvus. These treatments, followed by identical cooling and aging, enabled systematic evaluation of γ' dissolution, matrix supersaturation, reprecipitation kinetics, and their effects on microstructure and mechanical properties.

3.2 Microstructural Evolution During Solution Treatment

Solution treatment induced progressive recovery, static recrystallization, and γ' dissolution, with pronounced effects on grain structure and precipitate distribution (Fig. 3). At sub-solvus Temperature 1055 °C (Fig. 3-a) the deformed microstructure underwent substantial restoration, yielding a more homogeneous grain size distribution with equilibrium triple junctions. Fine-grained areas (FGAs arrows in Fig. 3) persisted as clusters of fine γ' precipitates (<1–3 μm), occupying ≈15% of the microstructure and exhibiting local enrichment in Al and Ti (confirmed by EDS). These FGAs displayed markedly higher hardness (490 ± 11 HV) compared to the surrounding matrix (380 ± 10 HV), reflecting their high γ' volume fraction. FGAs also can be seen on other solution temperatures at 1075°C (Fig. 3-b) and 1095°C (Fig. 3-c) but completely disappeared at 1115°C Solution treatment (Fig. 3-d).

Increasing solution temperature progressively reduced FGA volume fraction and hardness: to ≈9% and 461 ± 9 HV at 1075 °C, and <4% and 450 ± 7 HV at 1095 °C (Fig. 4). This evolution reflects gradual dissolution of γ' precipitates and redistribution of γ'-forming elements. FGAs originated from heterogeneous deformation features (shear bands and deformed grain boundaries) that acted as preferred

[DOI: 10.22068/ijmse.4669]

sites for localized γ' precipitation during cooling. The presence of residual precipitates may have contributed to restricting grain-boundary migration and grain growth up to 1095 °C through a possible pinning effect [15,17]. At 1115°C (super-solvus), complete dissolution eliminated this pinning effect, resulting in rapid grain coarsening to ≈94 μm and a slight hardness decrease.

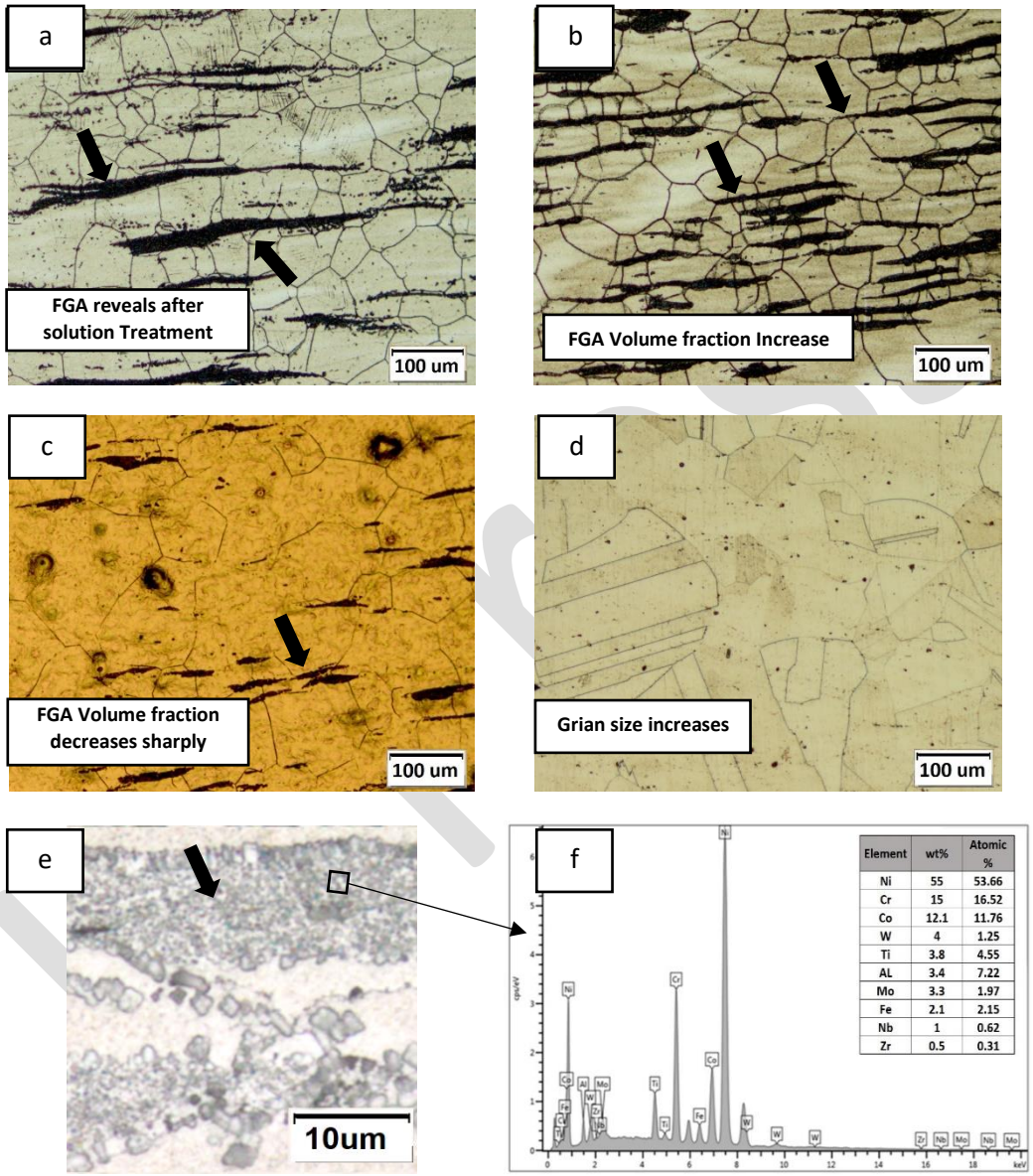

Fig. 3. Optical micrographs After solution-treated: (a) 1055 °C, (b) 1075 °C, (c) 1095°C, (d) 1115 °C; (e) higher-magnification view of FGA (Arows), (f) EDS spectrum from FGA.

The hardness changes resulting from the combined effects of recovery/recrystallization, γ′ evolution, FGA dissolution, and grain growth can be seen in Fig. 5. The matrix hardness decreases from the as-rolled condition to 1055 °C because Solution treatment cause to recovery and recrystallization reduce

[DOI: 10.22068/ijmse.4669]

the deformation-induced dislocation density. It then increases gradually up to 1095 °C, which is associated with progressive γ′ dissolution, redistribution of strengthening elements (Ti. Al, Nb) into the matrix, and the subsequent precipitation response. In contrast, the FGA hardness decreases continuously from about 490 HV at 1055 °C to about 445 HV at 1095 °C, indicating progressive dissolution and homogenization of these locally hard regions. At 1115 °C, the marked increase in grain size coincides with a reduction in matrix hardness, showing that grain-coarsening-induced softening becomes dominant. The observed microstructural changes are consistent with published work on the influence of solution treatment on recovery, recrystallization, precipitate dissolution, and grain-boundary mobility in nickel-based superalloys [1,2,15–18].

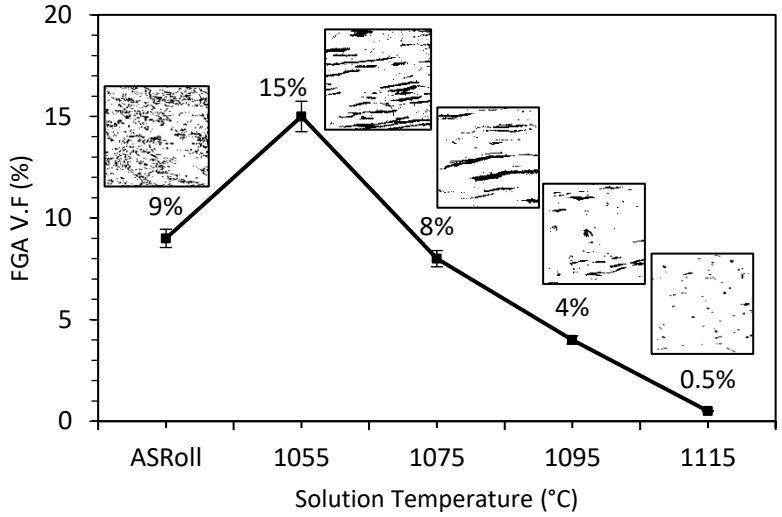

Fig. 4. Variation of FGA volume fraction with solution treatment temperatures compared to as roll condition with evidence from image analysis.

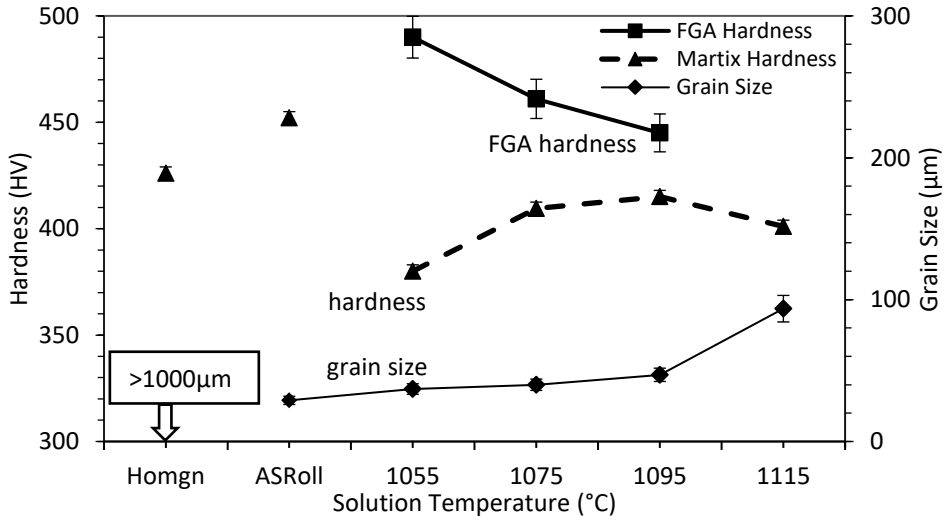

[DOI: 10.22068/ijmse.4669]

Fig. 5. Changes in average grain size, matrix hardness, and FGA hardness as a function of solution temperature (including data for homogenized and as-rolled conditions).

3.3 Evolution of γ′ Precipitates and High-Temperature Tensile Properties

Aging after solution treatment produced distinct γ' morphologies depending on the prior solution temperature (Fig. 6). At 1055 °C, heterogeneous precipitation persisted with precipitate-rich Fan-type regions (associated with FGAs) surrounded by γ'II-depleted zones, reflecting localized partitioning of Al and Ti. Higher solution temperatures at 1075°C, promoted progressive FGA dissolution, increasing matrix supersaturation and yielding a more uniform distribution of Spheroidal γ'II precipitates. The γ′-depleted regions appeared less pronounced at 1095 °C, indicating improved local microstructural homogeneity. Finally at 1115 °C, complete dissolution led to extensive reprecipitation but with coarser particles and reduced number density.

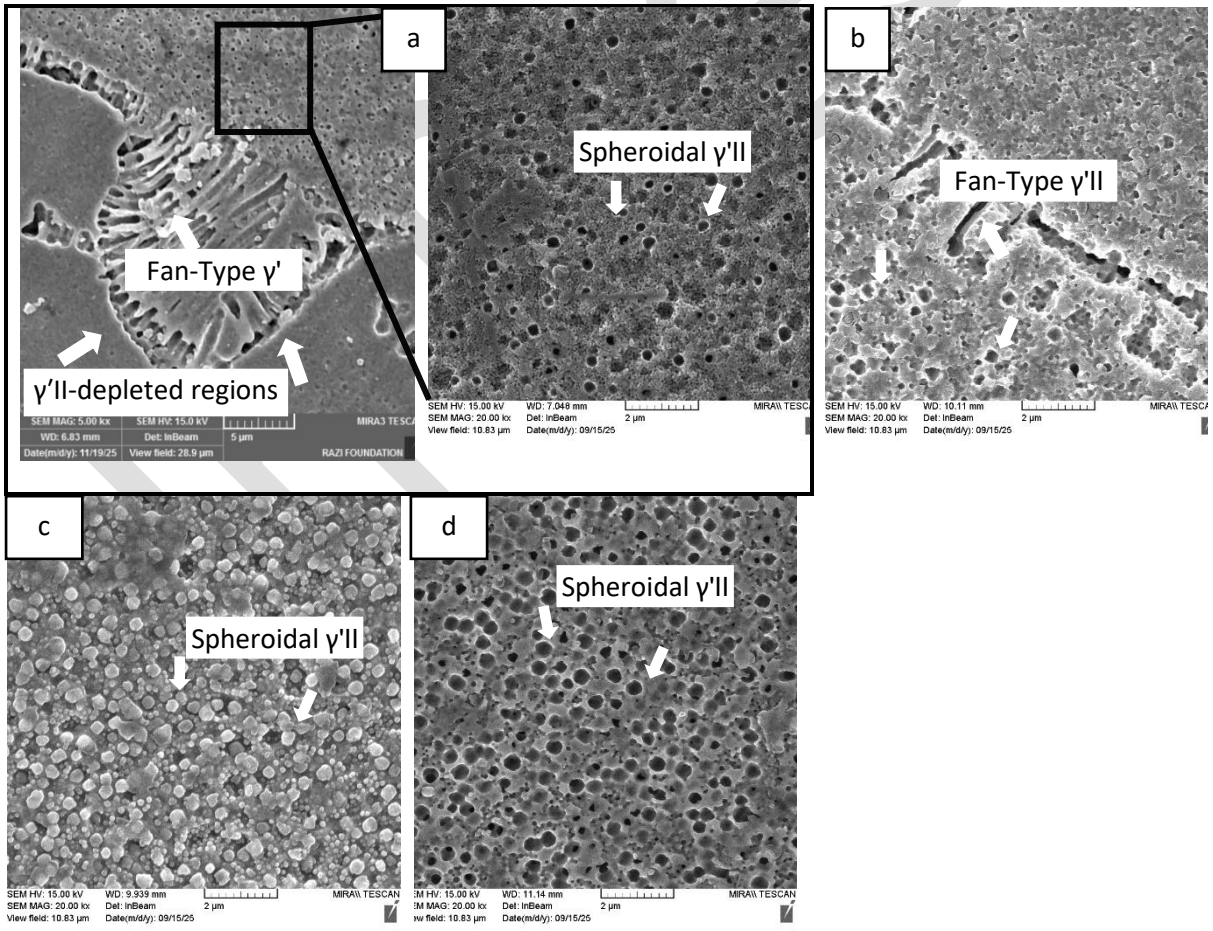

Fig. 6. FESEM micrographs showing the evolution of γ′II precipitate morphology after solution treatment at (a) 1055 °C with fan-type γ′II region and adjacent γ′II-depleted zones, (b) 1075 °C, (c) 1095 °C, and (d) 1115 °C.

[DOI: 10.22068/ijmse.4669]

Quantitative image analysis in Fig. 7 shows that increasing the solution-treatment temperature significantly alters both the amount and size of secondary γ′ precipitates. The measured γ′ volume fraction increases from approximately 12% at 1055 °C to a maximum of about 29% at 1095 °C, which can be attributed to progressive dissolution of primary γ′ and the resulting enrichment of the γ matrix with Al and Ti available for reprecipitation during subsequent cooling and aging. Meanwhile, the average secondary γ′ size increases continuously from approximately 55 nm at 1055 °C to about 260 nm at 1115 °C. At 1115 °C, however, the secondary γ′ volume fraction decreases slightly despite the pronounced increase in particle size, indicating that the precipitation response shifts toward fewer and considerably coarser precipitates rather than a further increase in their measured volume fraction. Thus, the results suggest that higher solution temperatures progressively favor γ′ growth and coarsening, with the most pronounced change occurring after treatment at 1115 °C [10,15].

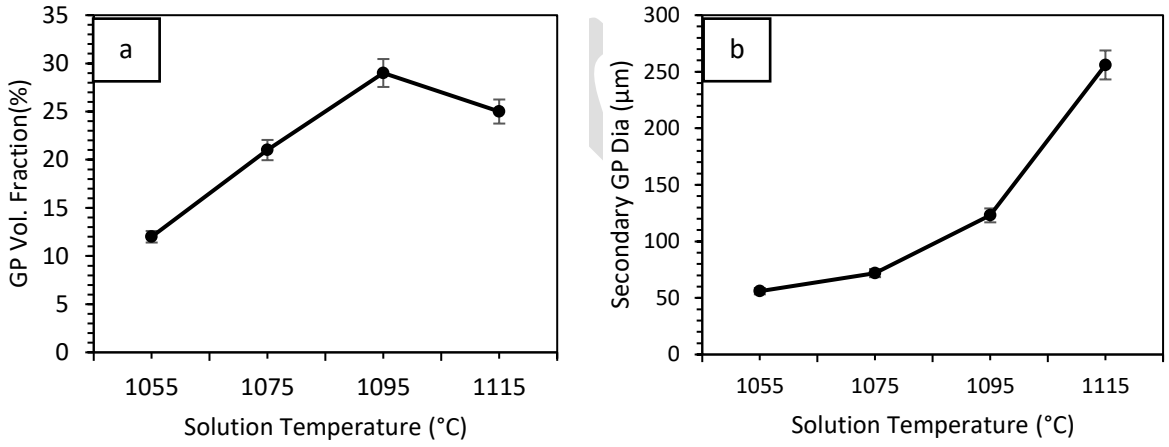

Fig. 7. Evolution of secondary γ' precipitate a) volume fraction and b)average size with solution temperature.

Tensile testing at 650 °C revealed properties generally comparable to literature values for René 65 [3,4,20], although the present hot-rolled material showed higher ductility (Fig. 8). Yield strength (YS) and ultimate tensile strength (UTS) were highest after solution treatment at 1055 °C, attributable to the fine precipitate population and residual FGA networks that enhanced resistance to dislocation motion. However, microstructural heterogeneities limited ductility (elongation ≈26%).

[DOI: 10.22068/ijmse.4669]

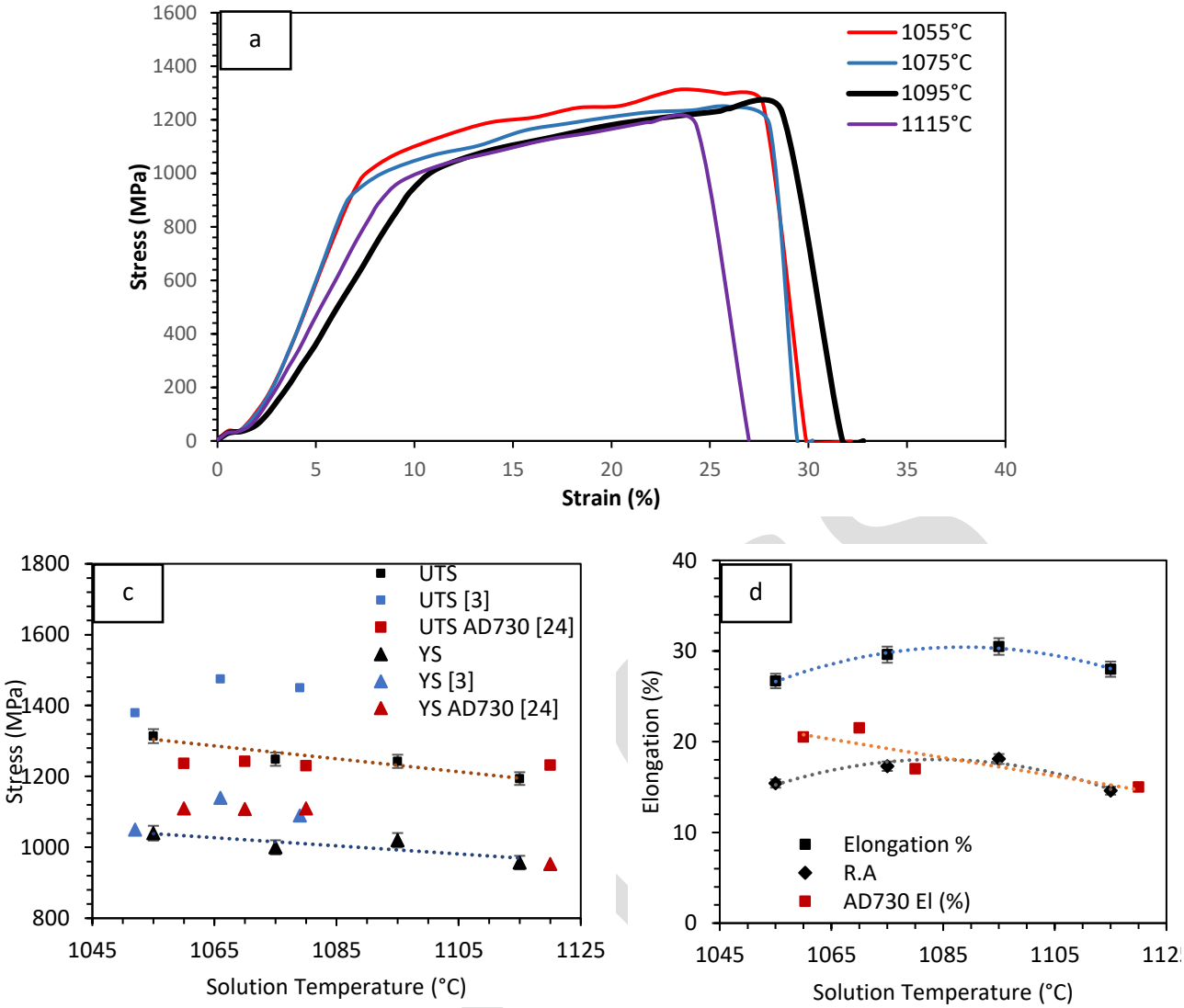

Fig. 8. (a) Tensile stress-strain curves (650 °C, 0.1(S^{-1})), (b) YS and UTS, (c) elongation and reduction in area as functions of solution temperature compared to [3, 20].

The optimal balance occurred at 1095 °C, where elimination of most FGA heterogeneities produced a uniform γ' distribution, yielding YS ≈1020 MPa and UTS ≈1242 MPa with elongation ≈31%. This improvement resulted from the reduction of local hardness gradients and increased deformation compatibility. At 1115 °C, precipitate coarsening combined with grain growth reduced strength (YS ≈957 MPa, UTS ≈1191 MPa) through diminished Hall–Petch strengthening and a shift in operative strengthening mechanisms—from weak/strong pair coupling toward Orowan bypassing for larger, non-shearable precipitates. Precipitation strengthening remains dominant in René 65, with efficacy depending critically on precipitate size, spacing, volume fraction, and spatial homogeneity [3,21].

[DOI: 10.22068/ijmse.4669]

3.4 Creep Behavior and Failure Mechanisms

Creep-rupture testing at 730 °C/530 MPa shows that solution treatment strongly controls creep performance through its effect on γ′ distribution, FGA stability, and grain structure. The 1055 and 1075 °C conditions exhibited short creep lives and limited steady-state deformation because residual FGA regions, local γ′-depleted zones, and associated microstructural heterogeneity promoted strain localization and early crack initiation. The 1095 °C specimen survived more than 100 h without rupture and exhibited the lowest minimum creep rate among the investigated conditions, indicating substantially improved creep resistance. Since the test was terminated before rupture, this value represents a run-out condition and not an actual rupture life. Therefore 1095 °C condition showed the lowest minimum creep rate beyond 100 h (>100 h) without rupture with about 11.9% creep elongation, indicating a more favorable balance between γ′ strengthening, reduced local heterogeneity, and microstructural stability. At 1115 °C, creep resistance deteriorated again despite greater γ′ dissolution, mainly because pronounced grain growth and coarsening reduced grain-boundary strengthening and facilitated creep deformation. Similar effects of γ′ stability, grain size, and heat-treatment condition on creep behavior have been reported for René 65 and related Ni-base superalloys [1,3,4,6,10,15,17].

The exceptional creep resistance at 1095 °C is attributed to several synergistic mechanisms, including a more uniform secondary γ′ distribution, reduced hardness gradients and γ′-depleted zones, and redistribution of the FGA regions. As indicated by the arrows in Fig. 10(c,d), the FGA regions become more dispersed after treatment at 1095 °C, reducing the severe local heterogeneity observed at lower solution temperatures. In addition, residual precipitates contribute to grain-boundary and annealing-twin pinning (Marked by arrows in Fig. 10(d)), thereby improving microstructural stability during creep exposure [13,22].

[DOI: 10.22068/ijmse.4669]

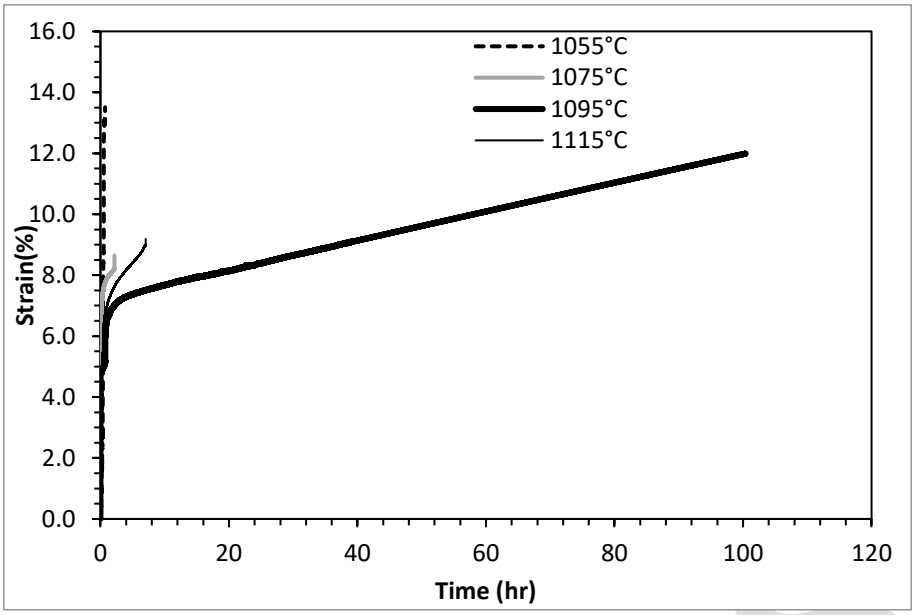

Fig. 9. Creep strain vs. time curves at 730 °C / 530 MPa.

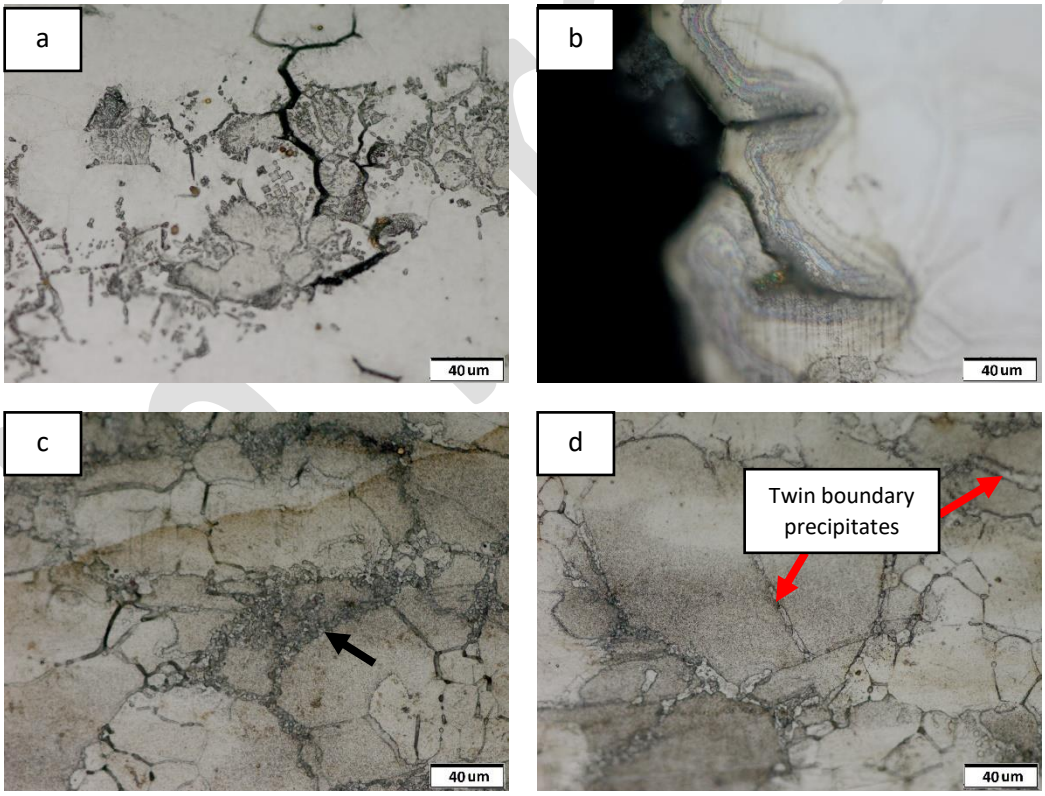

Fig. 10. Post-creep microstructures showing crack paths in samples solution-treated at (a) 1055 °C and (b) 1075 °C, and (c,d) redistribution of FGA regions in the 1095 °C sample.

Post-creep examination (Fig. 10) shows that the poor creep resistance of the 1055 and 1075 °C conditions is associated with crack initiation and propagation along heterogeneous FGA/matrix regions,

[DOI: 10.22068/ijmse.4669]

where local γ′ depletion promotes strain localization. At 1095 °C, the FGA regions become more dispersed, as indicated by the arrows in Fig. 10(c,d), while the more homogeneous γ′ distribution reduces local deformation and improves microstructural stability during creep. This reduced microstructural heterogeneity contributes to the improved creep resistance observed at 1095°C [1,2,6] and the observed crack morphology suggests that local microstructural heterogeneity may influence crack propagation paths.

Fig. 11 clearly demonstrates the strong dependence of creep behavior on solution temperature. The 1095 °C condition exhibits the lowest minimum creep rate and the longest creep life, confirming that a relatively homogeneous γ′ distribution and reduced FGA-related heterogeneity provide the most stable microstructure during creep. At 1115 °C, the minimum creep rate increases and creep life decreases markedly, which is attributed to pronounced grain growth and γ′ coarsening, reducing the effectiveness of both grain-boundary and precipitation strengthening. Thus, the results indicate that creep resistance depends on the combined stability of the γ′ distribution, FGA regions, and grain structure rather than on precipitate or grain size alone [1,3,6,10,15].

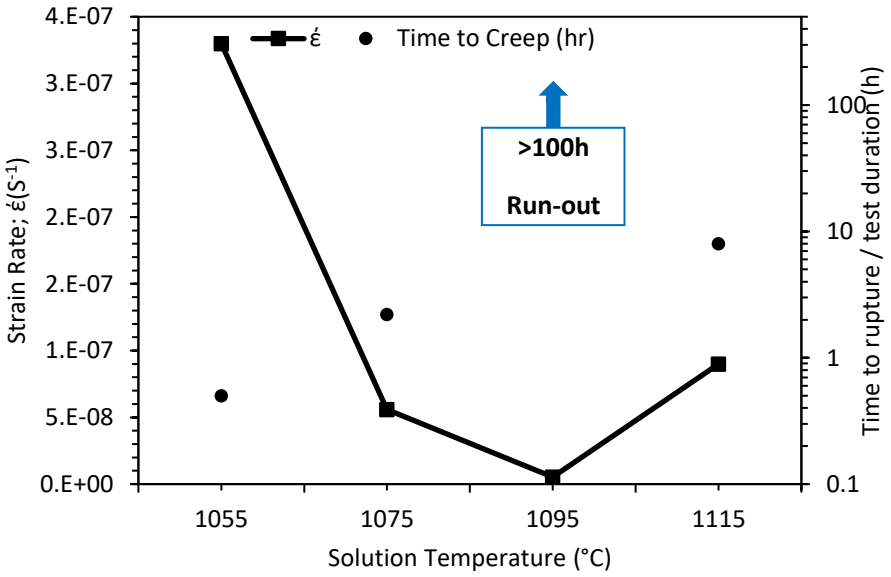

Fig. 11. Steady-state creep rate and time to rupture/test duration as functions of solution-treatment temperature. (1095 °C condition was terminated after 100 h without rupture and is therefore reported as a run-out condition.)

Conclusions

The effect of solution-treatment temperature on the microstructure, tensile properties, and creep

[DOI: 10.22068/ijmse.4669]

behavior of hot-rolled René 65 was systematically evaluated. The main conclusions are as follows:

1. Hot rolling produced pronounced deformation heterogeneity and FGA regions associated with localized γ′ precipitation. Their fraction decreased progressively with increasing solution-treatment temperature, from about 15% at 1055 °C to approximately 4% at 1095 °C, and was nearly eliminated at 1115 °C.
2. Increasing the solution temperature promoted progressive dissolution and redistribution of γ′-forming elements, resulting in a more homogeneous secondary γ′ distribution. However, treatment at 1115 °C caused substantial grain growth and marked γ′ coarsening.
3. The 1095 °C condition provided the most favorable balance between FGA reduction, γ′ homogeneity, grain-size stability, tensile strength, and ductility. At this condition, YS and UTS were approximately 1020 and 1242 MPa, respectively, with an elongation of about 31%.
4. The creep response showed a strong dependence on solution-treatment temperature. The 1095 °C specimen exhibited the lowest minimum creep rate and remained unfailed beyond 100 h at 730 °C/530 MPa, whereas both lower-temperature conditions and the 1115 °C condition showed inferior creep performance.
5. Overall, solution treatment at 1095 °C followed by aging at 760 °C for 8 h appears to provide the most suitable processing condition among those investigated, because it reduces FGA-related microstructural heterogeneity without inducing the excessive grain growth and γ′ coarsening observed at 1115 °C.

Declaration of open AI and AI-assisted technologies

The authors declare that no generative AI or AI-assisted technologies were used in the writing process of this manuscript. The declaration does not apply to use of basic tools, such as tools used to check grammar and spelling.

Acknowledgment

The authors would like to thank the materials research group for their work on casting, remelting, and hot rolling.

References

[1] Reed, R. C., The Superalloys: Fundamentals and Applications, Cambridge University Press, Cambridge, UK, 2006, 234-256.

[DOI: 10.22068/ijmse.4669]

[2] Pollock, T. M. and Tin, S., "Nickel-Based Superalloys for Advanced Turbine Engines: Chemistry, Microstructure and Properties," J. Propuls. Power, 2006, 22, 361–374.

[3] Wessman, A. E., Physical Metallurgy of Rene 65, a Next-Generation Cast and Wrought Nickel Superalloy for Use in Aero Engine Components, Doctoral Dissertation, University of Cincinnati, Cincinnati, USA, 2016.

[4] Heaney, J. A., Lasonde, M. L., Powell, A. M., Bond, B. J. and O'Brien, C. M., "Development of a New Cast and Wrought Alloy (René 65) for High Temperature Disk Applications," Proceedings of the 8th International Symposium on Superalloy 718 and Derivatives, TMS, 2014, 67–77.

[5] Katsari, C. M., Thermomechanical Processing Optimization of Rene 65 Turbine Engine Components via Heat Treatment Experimental Design, Ph.D. Thesis, McGill University, Montreal, Canada, 2021.

[6] Yao, Z., Zhou, B., Yao, K., Wang, H., Dong, J. and Davey, T., "Influence and Sensitivity of Temperature and Microstructure on the Fluctuation of Creep Properties in Ni-Base Superalloy," Materials, 2020, 13, 4758.

[7] Vasishta, A., Microstructural Design and Optimization of Nickel-Based Superalloys for Gas Turbines, Degree Project in Materials Science and Engineering, KTH Royal Institute of Technology, Stockholm, Sweden, 2023.

[8] Sims, C. T., Stoloff, N. S. and Hagel, W. C., Superalloys II, John Wiley & Sons, New York, USA, 1987.

[9] Katsari, C. M., Katnagallu, S. and Yue, S., "Microstructural Characterization of Three Different Size of Gamma Prime Precipitates in Rene 65," Mater. Charact., 2020, 169, 110542.

[10] Papadaki, C., Li, W. and Korsunsky, A. M., "On the Dependence of γ′ Precipitate Size in a Nickel-Based Superalloy on the Cooling Rate from Super-Solvus Temperature Heat Treatment," Materials, 2018, 11, 1528.

[11] Rae, C. M. F. and Reed, R. C., "Primary Creep in Single Crystal Superalloys: Origins, Mechanisms and Effects," Acta Mater., 2007, 55, 1067–1081.

[12] Katsari, C. M., Che, H., Turner, B., Wessman, A. and Yue, S., "Precipitation Characteristics of Gamma Prime Precipitate in Rene 65," Proceedings of the Materials Science and Technology Conference and Exhibition 2017 (MS&T17), Pittsburgh, USA, 2017, 1375–1381.

[DOI: 10.22068/ijmse.4669]

[13] Crudden, D., A Nickel-Based Alloy, US Patent Application US20220259702A1, 2022.

[14] Durand, M., Analyse des Mécanismes Métallurgiques Survenant dans l'Alliage AD730TM au Cours du Revenu de Relaxation des Contraintes, Doctoral Dissertation, Mines Paris–PSL, Paris, France, 2021.

[15] Alvarado, K., Janeiro, I., Florez, S., Flipon, B., Franchet, J.-M., Locq, D., Dumont, C., Bozzolo, N. and Bernacki, M., "Dissolution of the Primary γ′ Precipitates and Grain Growth during Solution Treatment of Three Nickel Base Superalloys," Metals, 2021, 11, 1921.

[16] Qiao, S., Liu, S., Li, N., Gao, X., Wen, X., Wang, F. and Yuan, C., "Abnormal Grain Growth in the Ni-Based Wrought Superalloy GH4698 Bar during Heat Treatment," J. Mater. Res. Technol., 2024, 30, 6563–6575.

[17] Liu, Y., Wang, M., Sun, P., Yang, G., Song, W. and Wang, X., "Effect of Solution Treatment on Microstructure Evolution of a Powder Metallurgy Nickel Based Superalloy with Incomplete Dynamic Recrystallization Microstructure," Metals, 2023, 13, 239.

[18] Xu, G., Wu, C., Liu, Z., Wang, Y., Zhang, Z., Li, Y. and Hu, P., "Effects of the Solution Treatment on Microstructural Evolution, Mechanical Properties, and Fracture Mechanism of Nickel-Based GH4099 Superalloy," J. Miner. Mater. Charact. Eng., 2021, 9, 566–589.

[19] Semiatin, S. L., Mahaffey, D. W., Tung, D. J., Zhang, W. and Senkov, O. N., "A Comparison of the Plastic-Flow Response of a Powder-Metallurgy Nickel-Base Superalloy Under Nominally-Isothermal and Transient-Heating Hot-Working Conditions," Metall. Mater. Trans. A, 2017, 48, 1864–1879.

[20] Devaux, A., Picqué, B., Gervais, M. F., Georges, E., Poulain, T. and Héritier, P., "AD730™—A New Nickel-Based Superalloy for High Temperature Engine Rotative Parts," Proceedings of Superalloys 2012, TMS, 2012, 911–919.

[21] Sondhi, S. K., Wei, D. and Henry, M. F., "Microstructure & Property Modeling in Ni-Base Superalloys," Proceedings of the 3rd International Conference on Multiscale Materials Modeling, Symposium 4: Microstructural Effects on the Mechanics of Materials, Freiburg, Germany, 2006, 547–550.

[22] Manna, S., Chan, H., Ghosh, A., Chakrabarti, T. and Sankaranarayanan, S. K. R. S., "Understanding and Control of Zener Pinning via Phase Field and Ensemble Learning," Comput. Mater.

[DOI: 10.22068/ijmse.4669]

Sci., 2023, 229, 112384.

[DOI: 10.22068/ijmse.4669]

Table 1- Chemical composition of the Rene 65 superalloy used (weight percent).

Eleme	Ni	Cr	Mo	W	Co	Fe	Nb	Ti	Al	P	S	N	O
Wt%	54.9	16.3	4.0	4.1	13.0	1.1	0.5	3.7	2.2	<0.00	<0.00	0.007	0.01

[DOI: 10.22068/ijmse.4669]